(Received 6 May 2024, Accepted 5 July 2024, Scheduled 16 July 2024)

Inclination Detection of Multi-Mode Orbital Angular Momentum Based on Multi-Label Class-Specific Lightweight Neural Network

Hui Yang, Yifei Cheng*, Zhong Yu, Zhe Wang, and Yi Lu

School of Communication and Information Engineering, Xi'an University of Posts & Telecommunications, Xi'an 710121, China

ABSTRACT: Orbital angular momentum (OAM) becomes a new resource for wireless communication due to the different modes being orthogonal. In OAM-based wireless communications, factors such as tilt and multipath distort the phase of the OAM beam, making the mode difficult to detect. We propose a multi-label class-specific lightweight neural network (MCSLNN) to measure tilt and detect mode from a single image. MCSLNN utilizes the MobileNetV2 network as the backbone feature extraction network, considering the terminal devices with limited computing resources. To improve the performance of multi-label classification, MCSLNN employs residual class-specific attention (CSRA) as the classification layer. Furthermore, MCSLNN employs the beam steering method to verify the correctness of the measured tilt. The network measures the tilt angle with an accuracy of 76% and an estimation error of $\pm 1^\circ$ in a validation experiment. Finally, we analyze the network's generalization from varying heights above the ground for reflection paths. The results indicate that MCSLNN is adaptable to diverse circumstances, thus making it suitable for 6G communication and radar applications.

1. INTRODUCTION

Orbital angular momentum (OAM) becomes a new resource for communication following time, frequency, space, and code type. OAM enables multiplexed mode with its orthogonal and infinite eigenmodes, thereby improving the spectrum utilization and capacity of the communication system [1]. The University of Southern California team realized 4-way multiplexed OAM beam transmission, achieving a transmission rate of 32 Gbit/s [2]. The Nippon Telegraph and Telephone Public Corporation (NTT) team studied a dual-polarization OAM-MIMO multiplexing system and realized the wireless transmission of 21 data streams at 201.5 Gbit/s in the 28 GHz band [3].

The key to realizing wireless OAM wave communication is accurately detecting the received OAM modes. For mode detection of OAM in the RF domain, modes based on single-point method [4], phase gradient method [4–6], and dynamic mode decomposition (DMD) method [7, 11] have been developed. The phase gradient method detects individual OAM modes by calculating the phase difference between two points and measuring the angle [4]. The DMD method takes the azimuthal sequence of the OAM beam as input. The method obtains the number of cycles that in the azimuthal direction along the OAM beam in the range of 2π, detecting single or multiple OAM modes [7]. The development of machine learning technology has prompted some scholars [8–10] to apply this method to the mode detection of vortex beams in the optical field. The multipath effect in real transmission has not been studied in the above literature.

Wireless OAM wave communication faces a significant challenge in that misaligned transmitting and receiving antennas cause mode crosstalk. The crosstalk will turn a single mode into a superposition of several modes. Certain researchers have proposed methods to address misalignment, including spectrum iteration [12] and beam steering [13, 14]. Among these methods, beam steering method is a relatively established approach. Moreover, tilt measurement is a necessary prerequisite to utilize the method. Subsequently, Gao et al. [15] noted that the phase profile of a titled OAM beam can indicate the inclination between the transmitter and receiver. Accordingly, they introduced an image processing technique for measuring the inclination of the OAM beam. Recently, Sun et al. proposed a recurrent neural network (RNN) model for measuring the inclination information of OAM beams inspired by the amplitude profile's sequential features after tilt [16]. The tilt measurement methods most study unidirectional tilt, while the tilts in the compound angular direction are common in actual communication. In addition, complex calculations can impede the application of previous measurement methods on terminal devices with limited computing resources.

In this letter, we propose a multi-label class-specific lightweight neural network (MCSLNN) that aims to reduce the limitations of the above methods. This paper establishes a two-dimensional inclination detection model as the tilt of compound angles is common in the actual environment, as shown in Fig. 1. Then, the backbone part of MCSLNN obtains feature tensor by training phase profiles containing tilt and mode information. MCSLNN can capture distinct spaces occupied by varying classes after passing the feature tensor

* Corresponding author: Yifei Cheng (13572500112@stu.xupt.edu.cn).

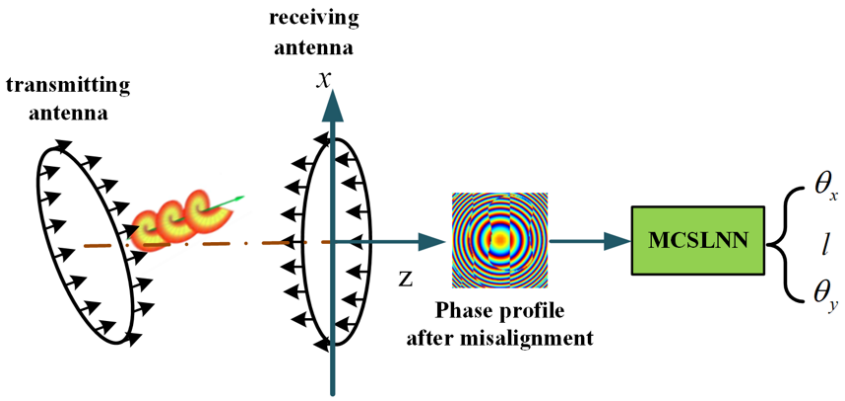

FIGURE 1. Flowchart for two-dimensional inclination detection.

through class-specific residual attention (CSRA) [17]. Next, we measure the tilt of a tilted multiplexed OAM beam at the experiment. Finally, we test network's generalization for reflection paths at different heights above the ground.

2. METHODOLOGY

2.1. Misalignment Transmission Model

One of the main methods of generating wireless OAM beams is the uniform circular array (UCA) with dipoles as array elements [18]. UCA controls phase through a phase shifter to produce multi-mode OAM beams. UCA can generate wireless OAM beams with modes between $-N/2$ and $N/2$ by feeding N array elements arranged at equal intervals with currents of equal amplitude and phase difference of $2\pi l/N$. Then, the electric field of UCA at any observation point $P(r,\theta,\varphi)$ in the space under the spherical coordinate system is expressed as [19]:

$$E(r,\theta,\varphi) = A_n \frac{e^{-ikr}}{r} \sum_{n=1}^{N} e^{ik\mathbf{Q}(\hat{\mathbf{x}},\hat{\mathbf{y}},\hat{\mathbf{z}})^T \cdot \mathbf{r}_n} e^{il\varphi_n}. \quad (1)$$

where l represents the mode of the OAM beam; $\varphi_n = 2\pi(n-1/N)$ $(n = 1,2,...,N)$ refers to the azimuth angle of the location of the UCA array element; $\mathbf{Q} = (\sin\theta\cos\varphi, \sin\theta\sin\varphi, \cos\theta)$ represents the location of the observation point; $k = 2\pi/\lambda$ denotes the wave number; and A_n denotes the amplitude excitation of the nth antenna array element.

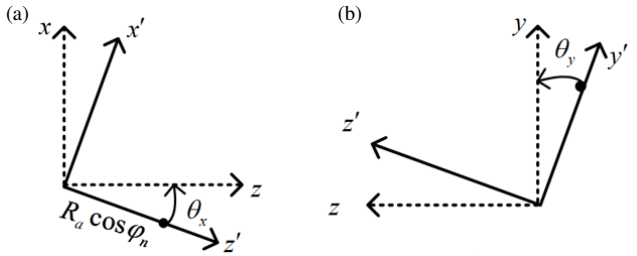

FIGURE 2. (a) Model of the horizontally inclined UCA array element. (b) Model of the vertically inclined UCA array element.

Set the tilted $x'y'z'$ coordinate system to rotate θ_x angle counterclockwise along the X-axis in the positive direction and rotate θ_y angle counterclockwise along the Y-axis to return to the original coordinate axis. Thus, the model for UCA misalignment is established, as illustrated in Fig. 2.

The position vector $\mathbf{r}_n$ of the tilted nth antenna element in the original coordinate system is transformed into:

$$\mathbf{r}_n = (\hat{\mathbf{x}},\hat{\mathbf{y}},\hat{\mathbf{z}})\left(\mathbf{X}'(\theta_x)\mathbf{Y}'(\theta_y)P_n\right). \quad (2)$$

where $P_n = R_a(\cos\varphi_n, \sin\varphi_n, 0)^T$ represents the position of the nth array element in the tilted coordinate system. R_a represents the radius of the transmitter array.

$$\mathbf{X}'(\theta_x) = \begin{bmatrix} \cos(\theta_x) & 0 & \sin(\theta_x) \\ 0 & 1 & 0 \\ -\sin(\theta_x) & 0 & \cos(\theta_x) \end{bmatrix}, \quad (3)$$

$$\mathbf{Y}'(\theta_y) = \begin{bmatrix} 1 & 0 & 0 \\ 0 & \cos(\theta_y) & \sin(\theta_y) \\ 0 & -\sin(\theta_y) & \cos(\theta_y) \end{bmatrix}. \quad (4)$$

where $\mathbf{X}'(\theta_x)$ is a rotational matrix that rotates along the X-axis by an angle of θ_x, and $\mathbf{Y}'(\theta_y)$ is a rotational matrix that rotates along the Y-axis by an angle of θ_y.

Multi-mode OAM is a linear superposition of different modal OAM beams [20]. Substituting (2), (3), and (4) into (1), the electric field of the tilted multi-mode OAM beam expresses as:

$$E_l = \sum_l A_n \frac{e^{-ikr}}{r} \sum_{n=1}^{N} \exp\left[ik\mathbf{Q}\left(\mathbf{X}'(\theta_x)\mathbf{Y}'(\theta_y)P_n\right) + il\varphi_n\right] \quad (5)$$

Then, Fig. 3(a) displays the phase profile in three composite angle situations based on (5).

At present, the mirror reflection model, depicted in Fig. 4, is the focus of research on multipath effects in wireless OAM beam communication systems. In the diagram, h represents the vertical distance between UCA and the ground.

According to the mirror theory [21], the OAM beam on the reflection path can be considered as the opposite mode OAM

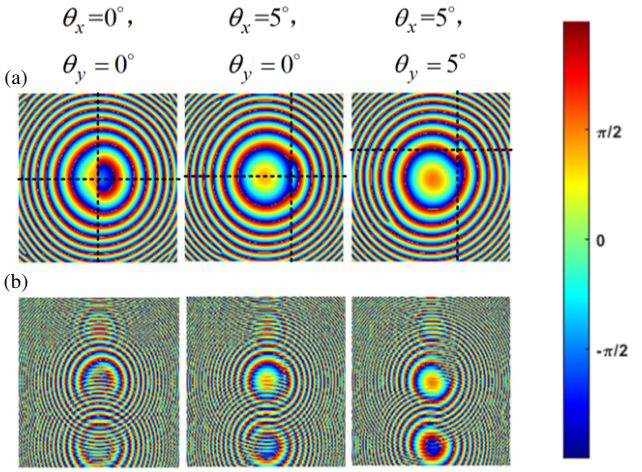

FIGURE 3. Profiles of multi-mode beams at different composite angles with a transmission distance of 200λ. (a) Phase profile of multi-mode OAM beams with $l = \pm 1$ and $l = \pm 2$. (b) Phase profile of multi-mode OAM beams with $l = \pm 1$ and $l = \pm 2$ at an antenna height h of 20λ above the ground.

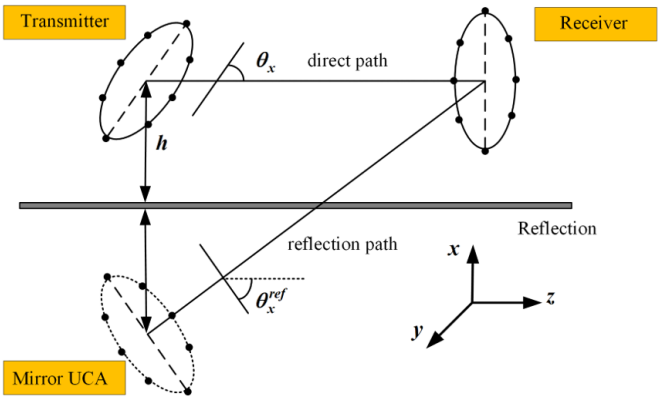

FIGURE 4. Transmission model of two-path UCA under misalignment.

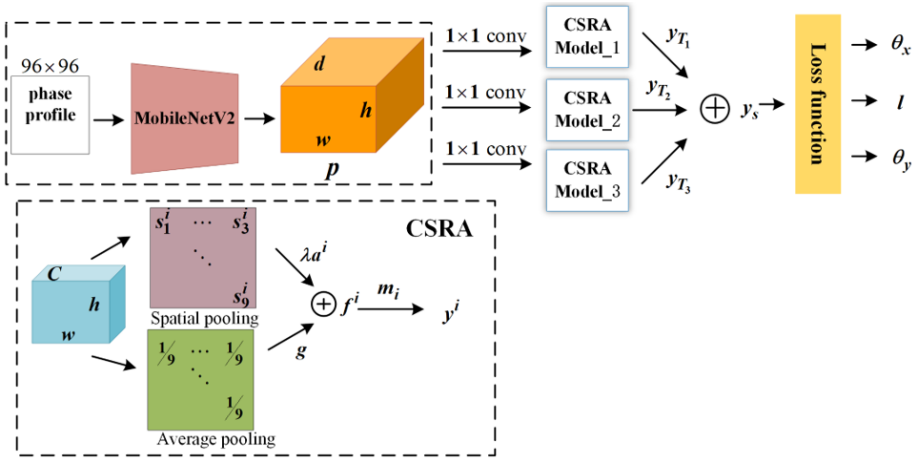

FIGURE 5. Structure of the proposed MCSLNN model.

beam emitted by the mirror transmitter UCA. Meanwhile, the rotational angles are mirrored as well, with the mirrored UCA having $\theta_x^{ref} = -\theta_x$ and $\theta_y^{ref} = -\theta_y$. Thus, we can derive the electric field expression of the multi-mode OAM beam in a two-path environment as

$$E_{two} = E_l + E_{-l}. \tag{6}$$

Fig. 3(b) displays the phase profile in different composite angle situations based on (6).

2.2. MCSLNN Structure

In this work, the MCSLNN structure can measure the tilt and detect the mode simultaneously, as shown in Fig. 5. We consider phase data as the image, where the position of the phase singularity displays tilt information, and the phase structure reflects mode information. The labels for mode classification and tilt classification in the misalignment model are not mutually exclusive; therefore, we treat them as a multi-label image classification problem. Multi-label classification can reduce the required amount of training data by enabling an image to contain both inclination and mode information.

The MCSLNN structure employs the MobileNetV2 [22] as the backbone network. MobileNetV2 is a lightweight convolutional neural network developed by the Google team. MobileNetV2 boasts a 20% reduction in parameters compared to its predecessor, MobileNetV1, while surpassing its accuracy. Like V1, V2 employs depth-separable convolutions to slim down the network. The computational workload comparison between deep separable convolution and regular convolution can be illustrated by (7).

$$\frac{P_D}{P_C} = \frac{1}{N_K} + \frac{1}{D_K^2} \tag{7}$$

where P_D represents the quantity of depth-separable convolutional computation, P_C the amount of ordinary convolutional

computation, D_K the size of the convolutional kernel, and N_K the number of channels in the output feature matrix.

In the MCSLNN structure's feature extraction stage, the feature extractor ϕ (MobileNetV2) processes the phase profile image I of the OAM beam, resulting in the feature tensor p of the image.

$$\mathbf{p} = \phi(I;\theta) \in \mathbb{R}^{d\times h\times w} \tag{8}$$

where d, h, and w represent the dimension, height, and width of the feature tensor, and θ denotes the parameter in the MobileNetV2 network. The size of the input phase profile image is 96×96 in this study. Therefore, the shape of the output feature tensor $\mathbf{p}$ is $1280 \times 3 \times 3$ after applying MobileNetV2 to the image. Then, the feature tensor $\mathbf{p}$ can be decoupled as $\mathbf{p}_1, ..., \mathbf{p}_9$ ($\mathbf{p}_i \in \mathbb{R}^{1280}$).

Single-label classification utilizes MobileNetV2 as the backbone network, and classification is typically executed via a fully connected (FC). While multi-label classification utilizes MobileNetV2 as the backbone network, using the FC leads to redundancy and mediocre classification results.

The MCSLNN structure introduces the concept of class-specific residual attention (CSRA) in the network classification layer. CSRA can capture the unique spatial regions occupied by various classes of objects, thus enhancing the performance of multi-label classification [17]. The class-specific attention score for the ith class ($i \in \mathbb{R}^3$) at the jth position ($j \in \mathbb{R}^9$) of the feature tensor $\mathbf{p}$ is:

$$s_j^i = \frac{\exp\left(T\mathbf{p}_j^T\mathbf{m}_i\right)}{\sum_{k=1}^{9}\exp\left(T\mathbf{p}_k^T\mathbf{m}_i\right)}, \tag{9}$$

where $\mathbf{m}_i \in \mathbb{R}^{1280}$ is the classifier for class i. T is the temperature that controls the sharpness of the score. The feature vector for each class is defined as a combination of feature tensors that are weighted by the spatial attention score s_k^i corresponding to class i.

$$\mathbf{a}^i = \sum_{k=1}^{9} s_k^i \mathbf{p}_k. \tag{10}$$

The CSRA algorithm employs global average pooling as the primary feature vectors $\mathbf{g}$ and $\mathbf{a}^i$ as the class-specific residual feature, as shown in Fig. 4. $\mathbf{a}^i$ is multiplied by a weight coefficient ($\lambda = 0.2$), and then $\mathbf{g}$ is added to obtain the residual attention feature $\mathbf{f}^i$ of the ith class:

$$\mathbf{f}^i = \mathbf{g} + \lambda\mathbf{a}^i = \sum_{k=1}^{9}\left(\frac{1}{9} + \lambda s_k^i\right)\mathbf{p}_k. \tag{11}$$

Submit all $\mathbf{f}^i$ to the classifier to obtain the single-head score vector $\mathbf{y}_{T_1}$.

$$\mathbf{y}_{T_1} = \left(y^1, y^2, \cdots, y^C\right) = \left(\mathbf{m}_1^T\mathbf{f}^1, \mathbf{m}_2^T\mathbf{f}^2, \cdots, \mathbf{m}_C^T\mathbf{f}^C\right), \tag{12}$$

where C represents the number of multilabel categorization categories. The score vectors from the H heads are added to produce the score vector for multi-head attention, which is identified as $\mathbf{y}_s$.

$$\mathbf{y}_s = \sum_{h=1}^{H}\mathbf{y}_{T_i} \tag{13}$$

In (13), T_i represents the temperature of the ith head.

Moreover, the MCSLNN structure employs the cross-entropy function as the model's loss function.

3. RESULTS AND DISCUSSION

3.1. Training Results and Verification of MCSLNN Structure

This work uses MATLAB to generate phase profile based on the functions in Section 2.1 with an observation window of $50\lambda \times 50\lambda$. A 16-element UCA is used to generate the mode group of $l_m = [(1,-1,2,-2),(1,-1,3,-3),(3,-3,7,-7),(4,-4,5,5),(1,3,5,7),(2,4,6,8),(-2,3,5,7),(-1,3,4,-6),(1,-2,2,-7),(2,-2,5,-5)]$ for a quadruple multiplexed OAM beam at 10 GHz. The radius of the transmitting UCA is 2λ.

We vary the transmission distance from 180λ to 220λ in steps of λ to enhance the robustness of the MCSLNN structure. The MATLAB generates ten types of four-mode phase profiles by changing the transverse inclination angle θ_x and longitudinal inclination angle θ_y from 1° to 10° in steps of 1°. The modes l of four-mode beam are taken as l_m. The dataset comprises 41,000 phase maps, with each map consisting of 96 by 96 pixels and a total of $100 \times 10 \times 41$ sheets. The ratio of validation set to test set is $9:1$. Training is performed in Pycharm using the Pytorch 1.13.1 on a computer with an Inter Core i5-10400H CPU. The batch size of training MCSLNN is 16; the initial learning rate of Adam optimization function is 0.001; and the number of iterations is 100.

The structure achieves a more than 95% accuracy rate in recognizing inclinations in compound angle after conducting 100 iterations, as shown in Fig. 6(a). The accuracy of multi-mode detection has surpassed 99%, as shown in Fig. 6(b). It is obvious that the proposed structure is more sensitive to global changes than to local changes. In comparison to alternative machine learning techniques, the precision of MCSLNN in detecting mode is on par with the most optimal outcomes, though it does not surpass 99.33%, as shown in Table 1. To verify the robustness of MCSLNN during inclination detection, additive Gaussian white noise is added to the test set. The accuracies of detection by MCSLNN under different SNRs are shown in Fig. 7. It is clear that the MCSLNN detects θ_x, l, and θ_y with accuracies of 96.3%, 98.5%, and 93.6% respectively at an SNR of 15 dB.

MCSLNN verifies the accuracy of the tilt measurements using the beam steering method. The beam steering vector $\mathbf{w}a$ is written as $\mathbf{w}_a = [1, \exp(-jW_2), ..., \exp(-jW_N)]$ at the receiver, where $W_n = kR_a(-\cos\varphi_n \sin\theta_x + \sin\varphi_n \sin\theta_y \cos\theta_x)$, $n = 1, ..., N$. By substituting the measured values of $\theta_x = 2°$ and $\theta_y = 3°$ into $\mathbf{w}_a$, we could obtain the corrected phase profile. The results are shown in Figs. 8(a) and (b). In addition, in a noisy environment, the phase can also be corrected using the tilt information obtained from the inclination detection, as shown in Figs. 8(c) and (d).

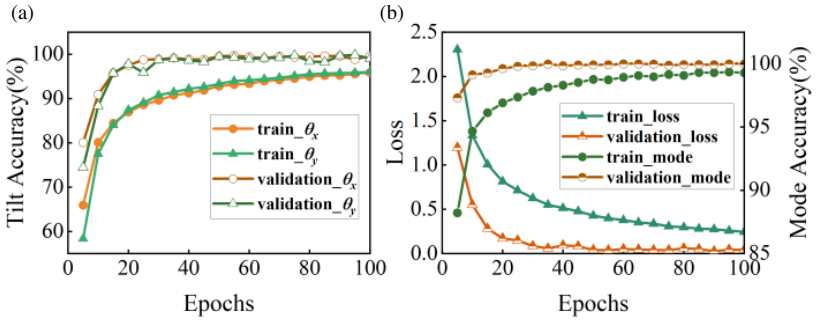

FIGURE 6. (a) Accuracy of tilt measurement. (b) Accuracy of mode detection and loss value of structure training.

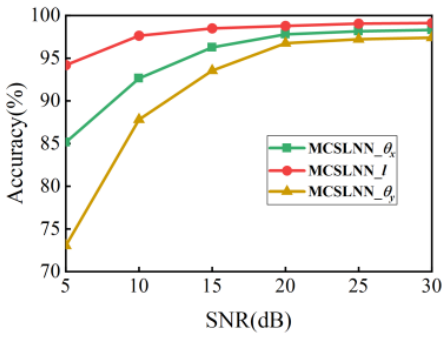

FIGURE 7. The accuracy of detecting θ_x, l and θ_y by MCSLNN under different SNR.

TABLE 1. Comparison of other methods for detecting tilt and mode.

Model	Accuracy_θ_x	Accuracy_l	Accuracy_θ_y
[8]	-	98.82%	-
[9]	-	99%	-
[10]	-	99.33%	-
[17]	99.1%	-	-
MCSLNN	95.6%	99.3%	96.1%

3.2. Experimental Setup

We examine the practical application performance of MCSLNN through an experiment. The experiment utilizes a 2×2 MIMO double helix dielectric resonator antenna (DRA) as the transceiver antenna, as shown in Fig. 9(a). The antenna generates four-way multiplexed OAM beams with $l = \pm 1$ and $l = \pm 3$ in two different frequency bands. The working frequency bands of the antenna are 1.78–3.02 GHz and 4.01–7.73 GHz. Next, a vector network analyzer (VNA) generates the 2.9 GHz and 6.1 GHz radio frequency (RF) signals. The computer controls the transmitter's mechanical arm to tilt at any angle between 1° and 10° perpendicular and parallel to the propagation direction, with an accuracy of 1°, as shown in Fig. 9(b). Finally, we collect the phase data of the multiplexed OAM beam passing through the low noise amplifier and mixer [23], totaling 200 samples.

The MCSLNN structure measures the received phase data and labels the inclination information on the phase profile.

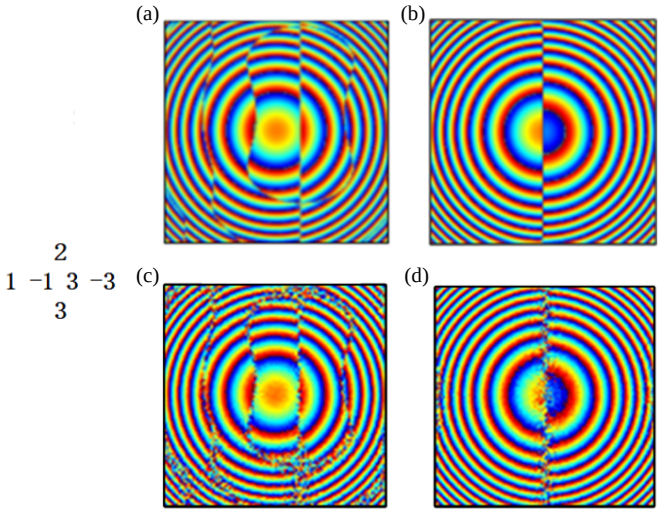

FIGURE 8. (a) The measurement result is the phase profile of $\theta_x = 2°$ and $\theta_y = 3°$. (b) Corrected phase profile. (c) Phase profile of the misalignment at 15 dB SNR. (d) Corrected phase profile at 15 dB SNR.

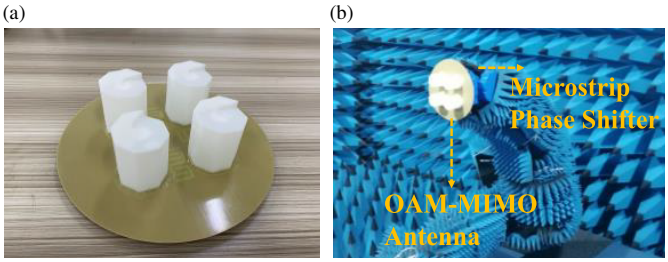

FIGURE 9. (a) 2×2 MIMO dual helix dielectric resonator antenna. (b) Anechoic chamber measurement system.

Then, the measured angle is used to adjust the beam steering vector for correction. The result shows that the accuracy of the measured tilt is 76%. We study the samples with incorrect measures and find that the measured values differ by $\pm 1°$ from the actual values.

3.3. Structure Testing under Two-Path

To validate the generalization of the MCSLNN structure on data sets with reflection paths, we compare MCSLNN with the MobileNetV2-FC structure. MobileNetV2-FC is a struc-

ture combining MobileNetV2 and FC, based on the general operation of multi-label classification. Then, the MobileNetV2-FC structure utilizes the multi-mode dataset presented in Section 3.1 to train.

The reflection path distorts the phase structure of the direct path is related to the height above the ground [21]. We using a test set which includes reflection paths and varying heights above the ground to compare the MCSLNN with MobileNetV2-FC. It is evident that due to the existence of class-specific structures, the MCSLNN model performs better than MobileNetV2-FC on test sets at different heights above the ground. The accuracy of both structures rises as the height above ground grows in Fig. 10. This trend is due to the center of the reflected path moving away from the center of the direct path as the antenna height increases above the ground.

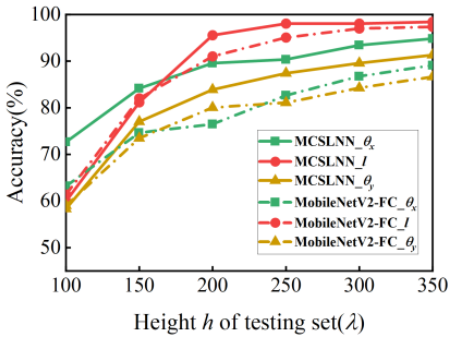

FIGURE 10. Performance comparison of different models on test sets at varying heights h above the ground.

4. CONCLUSION

In this study, we propose an MCSLNN structure for measuring compound tilt and detecting modes. By training the simulated multi-mode dataset, MCSLNN achieves accuracies of 95.9%, 96.1%, and 99.3% for measuring composite tilt and detecting modes, respectively. Next, MCSLNN utilizes double helix multiplex antennas for experiments. The experimental result shows that the accuracy of measuring inclination reaches 76%, and the estimation error is $\pm 1^{\circ}$. Subsequently, we compare MCSLNN and MobileNetV2-FC to verify the generalization in multipath cases. The results show that MCSLNN is suitable for multiple situations. Moreover, MCSLNN is appropriate for devices with limited computing resources due to low network parameters, showing great potential in OAM-based communications and radar applications. In future work, we will investigate the potential for real-time detection and integration with other communication systems, such as OAM shift keying systems.

ACKNOWLEDGEMENT

This work was supported by Pilot Project on Comprehensive Innovation and Reform of High-value Intellectual Property Rights for New-Generation Intelligent Communication Networks 2020IPYY/CG01.

REFERENCES

[1] Hu, T., Y. Wang, X. Liao, and J. Zhang, "OAM-based beam selection for indoor millimeter wave MU-MIMO systems," *IEEE Communications Letters*, Vol. 25, No. 5, 1702–1706, May 2021.

[2] Yan, Y., G. Xie, M. P. J. Lavery, H. Huang, N. Ahmed, C. Bao, Y. Ren, Y. Cao, L. Li, Z. Zhao, *et al.*, "High-capacity millimetre-wave communications with orbital angular momentum multiplexing," *Nature Communications*, Vol. 5, No. 1, 4876, Sep. 2014.

[3] Yagi, Y., H. Sasaki, T. Yamada, and D. Lee, "200 Gb/s wireless transmission using dual-polarized OAM-MIMO multiplexing with uniform circular array on 28 GHz band," *IEEE Antennas and Wireless Propagation Letters*, Vol. 20, No. 5, 833–837, May 2021.

[4] Mohammadi, S. M., L. K. S. Daldorff, K. Forozesh, B. Thidé, J. E. S. Bergman, B. Isham, R. Karlsson, and T. D. Carozzi, "Orbital angular momentum in radio: Measurement methods," *Radio Science*, Vol. 45, No. 4, 1–14, 2010.

[5] Cano, E. and B. Allen, "Multiple-antenna phase-gradient detection for OAM radio communications," *Electronics Letters*, Vol. 51, No. 9, 724–725, Apr. 2015.

[6] Xie, M., X. Gao, M. Zhao, W. Zhai, W. Xu, J. Qian, M. Lei, and S. Huang, "Mode measurement of a dual-mode radio frequency orbital angular momentum beam by circular phase gradient method," *IEEE Antennas and Wireless Propagation Letters*, Vol. 16, 1143–1146, 2017.

[7] Zhang, Y., M. L. N. Chen, and L. J. Jiang, "Analysis of electromagnetic vortex beams using modified dynamic mode decomposition in spatial angular domain," *Optics Express*, Vol. 27, No. 20, 27 702–27 711, Sep. 2019.

[8] Wang, X., Y. Qian, J. Zhang, G. Ma, S. Zhao, R. Liu, H. Li, P. Zhang, H. Gao, F. Huang, and F. Li, "Learning to recognize misaligned hyperfine orbital angular momentum modes," *Photonics Research*, Vol. 9, No. 4, B81–B86, Apr. 2021.

[9] Raskatla, V., P. S. Badavath, and V. Kumar, "Convolutional networks for speckle-based orbital angular momentum modes classification," *Optical Engineering*, Vol. 61, No. 3, 036 114–036 122, Mar. 2022.

[10] Chen, J., Q. Zeng, C. Li, Z. Huang, P. Wang, W. Xiong, Y. He, H. Ye, Y. Li, D. Fan, and S. Chen, "Orbital angular momentum mode demodulation with neural network-assisted coherent nanophotonic circuits," *Optics Communications*, Vol. 537, 129433, Jun. 2023.

[11] Zhang, Y. and L. Jiang, "Suppressing white-noise interference for orbital angular momentum waves via the forward-backward dynamic mode decomposition," *IEEE Transactions on Antennas and Propagation*, Vol. 71, No. 3, 2879–2884, Mar. 2023.

[12] Zhao, P., S. Li, Y. Wang, X. Feng, C. Kaiyu, L. Fang, W. Zhang, and Y. Huang, "Identifying the tilt angle and correcting the orbital angular momentum spectrum dispersion of misaligned light beam," *Scientific Reports*, Vol. 7, No. 1, 7873, Aug. 2017.

[13] Chen, R., H. Xu, M. Moretti, and J. Li, "Beam steering for the misalignment in UCA-based OAM communication systems," *IEEE Wireless Communications Letters*, Vol. 7, No. 4, 582–585, Aug. 2018.

[14] Chen, R., W.-X. Long, X. Wang, and J. Li, "Multi-mode OAM radio waves: Generation, angle of arrival estimation and reception with UCAs," *IEEE Transactions on Wireless Communications*, Vol. 19, No. 10, 6932–6947, Oct. 2020.

[15] Gao, X., X. Song, Z. Zheng, M. Xie, and S. Huang, "Misalignment measurement of orbital angular momentum signal based on spectrum analysis and image processing," *IEEE Transactions on*

Antennas and Propagation, Vol. 68, No. 1, 521–526, Jan. 2020.

[16] Sun, J.-J., S. Sun, L.-J. Yang, and J. Hu, "Enhanced misalignment estimation of orbital angular momentum signal based on deep recurrent neural networks," *IEEE Transactions on Antennas and Propagation*, Vol. 71, No. 6, 5522–5527, Jun. 2023.

[17] Zhu, K. and J. Wu, "Residual attention: A simple but effective method for multi-label recognition," in *Proceedings of the IEEE/CVF International Conference on Computer Vision (ICCV)*, 184–193, Oct. 2021.

[18] Yu, Z., Q. Gao, B. He, and L. Guo, "Effects of concentration, temperature, and geometry on double spiral liquid orbital angular momentum antenna," *IEEE Antennas and Wireless Propagation Letters*, Vol. 20, No. 12, 2506–2510, Dec. 2021.

[19] Liu, K., Y. Cheng, Z. Yang, H. Wang, Y. Qin, and X. Li, "Orbital-angular-momentum-based electromagnetic vortex imaging," *IEEE Antennas and Wireless Propagation Letters*, Vol. 14, 711–714, 2014.

[20] Chen, X., W. Xue, H. Shi, J. Yi, and W. E. I. Sha, "Orbital angular momentum multiplexing in highly reverberant environments," *IEEE Microwave and Wireless Components Letters*, Vol. 30, No. 1, 112–115, Jan. 2020.

[21] Wang, L., W. Park, C. Yang, H.-D. Brüns, D. G. Kam, and C. Schuster, "Wireless communication of radio waves carrying orbital angular momentum (OAM) above an infinite ground plane," *IEEE Transactions on Electromagnetic Compatibility*, Vol. 62, No. 5, 2257–2264, Oct. 2020.

[22] Sandler, M., A. Howard, M. Zhu, A. Zhmoginov, and L.-C. Chen, "Mobilenetv2: Inverted residuals and linear bottlenecks," in *The IEEE Conference on Computer Vision and Pattern Recognition*, 4510–4520, 2018.

[23] Xiong, X., S. Zheng, Z. Zhu, Y. Chen, H. Shi, B. Pan, C. Ren, X. Yu, X. Jin, W. E. I. Sha, and X. Zhang, "Experimental study of plane spiral OAM mode-group based MIMO communications," *IEEE Transactions on Antennas and Propagation*, Vol. 70, No. 1, 641–653, Jan. 2022.